Global Journal of Advanced Engineering Technologies and Sciences
[Thangavelan *et al*, 13(4): April, 2026] ISSN (Online): 2349-0292

DENSITY FUNCTIONAL THEORY AND MOLECULAR DOCKING STUDIES OF 2-(3, 4-DIHYDROXYPHENYL)-3,5,7-TRIHYDROXY-4-OXO-4H-CHROMEN-3-YL B-D-GLUCOPYRANOSIDE (5H1P1C4O1G)

Thangavelan Niruban Balu*[1], P. Venkatesh[2], Rajakumari Subramaniyan[3]
*[1]Department of Chemistry, Velammal Engineering College, Chennai, Tamil Nadu, India
[2]Department of Chemistry, Pachaiyappa's college, Chennai, Tamil Nadu, India
[3]Department of Chemistry, Vel Tech Multi Tech Dr. Rangarajan Dr. Sakunthala Engineering College, Chennai, Tamil Nadu, India
* E-mail: niruban.t@gmail.com

Received: 17/01/2025 **Revised**: 25/02/2026 **Accepted**: 23/03/2026

ABSTRACT

Flavonoid glycosides are significant pharmacologically relevant natural products that have not been studied sufficiently, and whose molecular interactions with cancer-related proteins are scarcely known. The bioactive flavonoid glycoside known to have antioxidant, anti-inflammatory and anticancer effects is 2-(3,4-dihydroxyphenyl)-3,5,7-trihydroxy-4-oxo-4H-chromen-3-yl 5H1P1C4O1G, which was not thoroughly studied in terms of its specific binding mechanisms The article employed molecular docking to determine important amino acid residues that stabilize the ligand and protein in this study that was conducted between 5H1P1C4O1G and cancer-associated proteins 3ERT, 6J90, and 7RPU. Of the targets analyzed, 3ERT had the highest binding affinity, which means it could be the most desirable anticancer target of the compound.

"Moreover, the electronic structure of the compound, its stability, and reactivity were assessed by means of the density functional theory (DFT) calculations at the B3LYP/6-311++G(d,p) level. Analysis of frontier molecular orbital, molecular electrostatic potential mapping and global reactivity descriptors gave a clue on the charge distribution and the reactive site that was involved in strong binding interactions. Altogether, the joint computational findings indicate that 5H1P1C4O1G has the best anticancer potential in 3ERT target, and can be used as a useful scaffold to develop multi-target anticancer agents."

KEYWORDS: 5H1P1C4O1G, 3ERT, 6J90, 7RPU anticancer activity, flavonoid glycoside.

DOI: https://doi.org/10.64149/gjaets.13.4.1-19

1. INTRODUCTION

Cancer is one of the major causes of death around the globe with the largest share of cancer incidents and mortality in the world being made up of cancer of the breast, lung, colorectal, pancreatic, and prostate cancers [1], [2]. These cancers are linked with intricate molecular heterogeneity, distorted signal transduction routes and, mutations, which foster tumor development, metastasis, and chemotherapy resistance [3], [4]. Although there has been consistent advancement in cancer diagnosis and targeted therapy, most of the anticancer drugs currently available are poorly selected, with side effects and most of them are developing resistance to drugs quite rapidly. Thus, the identification of novel bioactive molecules with enhanced pharmacological qualities continues to be a significant goal in the contemporary medicinal and pharmaceutical chemistry [5].

Natural polyphenolic compounds, in particular flavonoid and chromen-4-one derivatives, have gained much interest because of their broad-based biological properties, such as antioxidant, anti-inflammatory, antimicrobial, and anticancer properties [6]. The availability of numerous hydroxyl groups and conjugated aromatic systems of these molecules allows the strong intermolecular interactions with biological targets, and thus, they are good molecules to use in structure-based drug design. In this respect, the flavonoid glycoside 2-(3,4-dihydroxyphenyl)-3,5,7-trihydroxy-4-oxo-4H-chromen-3-yl 1-phosphoglucopyranoside (5H1P1C4O1G) is a polyhydroxylated chromen-4-one molecule with multiple

hydro These structural features indicate that this compound can serve as a possible lead molecule in the development of anticancer drugs.

Over the past few years, computational chemistry has been used to become an indispensable part of forecasting the biological activity of new compounds prior to experimental research. The analysis of molecular docking gives the data of the interactions between the ligands and proteins, but the density functional theory (DFT) also gives a comprehensive insight into the electronic structure, stability, and reactivity of the molecules. The docking and DFT techniques have been popularly combined to study the theoretical analysis of flavonoid-based compounds and to design new therapeutic agents rationally [7].

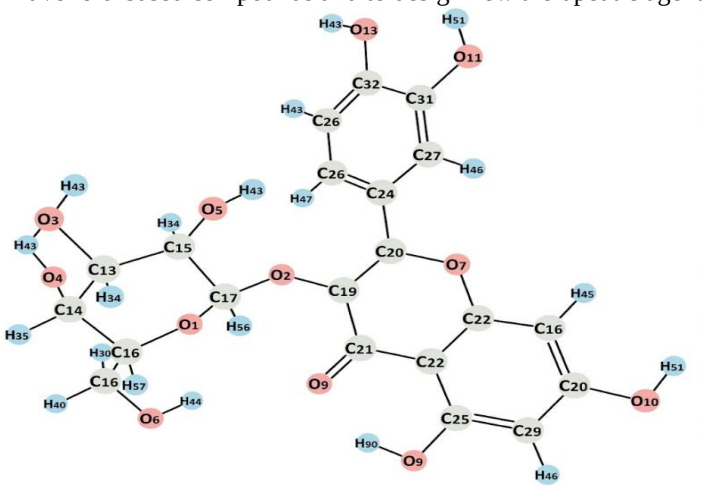

Fig. 1. Optimized molecular structure of 5H1P1C4O1G

2. MATERIALS AND METHODS

2.1. Identification of the Target Protein

The 3D crystal structures of the biomarkers that are related to cancer were extracted out of the protein database (PDB) through the use of the PDB IDs of 3ERT, 6J90, 7RPU and 8TSK and were used.

to perform the molecular docking analysis. The docking analysis was done using a version of Auto dock Tools, 1.5.7 [8]. All the ions, water molecules, co-crystallized ligands and ions were removed before docking. Thereafter, Kollman charges were added and polar hydrogen atoms were added. The generated protein structure was preserved in the form of the PDBQT format to be utilized in the future in molecular docking studies.

2.2. Ligand Retrieval and Optimization

A free chemical database had the molecular structure of 5H1P1C4O1G, which was utilized in computational studies. The substance was acquired commercially. Before docking analysis, the ligand geometry was optimized to yield a minimum-energy conformation. The assignment of Gasteiger charges, rotatable bond definition, and ligand were saved in PDBQT format by Auto Dock Tools (version 1.5.7) [9].

2.3. Molecular Docking Protocol

Auto Dock with Lamarckian genetic algorithm was conducted to perform the molecular docking simulations [10]. The docking grid box was established to cover the active binding sites of the 3ERT, 6J90, 7RPU, and 8TSK with dimensions that were adequate to allow complete ligand flexibility inside the binding pocket. The default auto-dock parameters were used unless otherwise. Several docking cycles were carried out to produce a variety of binding arrangements. The top-ranked docked poses were then selected according to the anticipated binding energy and the most energetically favorable structure was chosen to be further analyzed in terms of interactions through the usage of molecular visualization software [11].

2.4. Density Functional Theory Calculations

"Density functional theory (DFT) calculations were used to study the electronic structure and reactivity properties of 5H1P1C4O1G. Geometry optimization was done using 6-311++G(d,p) basis set and B3LYP exchange-correlation functional [12]. All computations were done in the gas phase and no symmetry constraints were applied. The energies of the frontier molecular orbitals, including the HOMO

and LUMO were calculated and the HOMO- LUMO gap was evaluated. To have a better insight into the molecular docking data, global reactivity descriptors have been produced in order to shed light on the chemical stability and interaction potential of 5H1P1C4O1G."

Table 1. Theoretical values of bond lengths and angles for this compound 5H1P1C4O1G. (Å: angstrom unit, °:degree.)

Bond Length (Å)	DFTB3LYP/6–311++G (d,p)	Bond Length (Å)	DFTB3 LYP/6–311++G (d,p)	Bond Angle (Å)	DFTB3LYP/6–311++G (d,p)	Bond Angle (Å)	DFTB3LYP/6–311++G (d,p)	Bond Angle (Å)	DFTB3LYP/6–311++G (d,p)	Bond Angle (Å)	DFTB3 LYP/6–311++G (d,p)
O1-C16	1.438	C16-C18	1.52	C16-O1-C17	112.9	O6-C18-H40	107.5	C13-C15-C17	109.3	C30-C26-H45	122.2
O1-C17	1.402	C16-H37	1.099	O1-C16-O4	108.7	C23-O7-C20	121.7	C13-C15-H36	109.3	C26-C30-C29	121.9
O2-C17	1.422	C17-H38	1.097	O1-C16-C18	105.6	O7-C23-C22	120.4	C16-C14-H35	109	H46-C27-C31	118.3
O2-C19	1.372	C18-H39	1.099	O1-C16-H37	109.4	O7-C23-C26	116.8	C14-C16-C18	115.1	C27-C31-C33	119.6
O3-C13	1.425	C18-H40	1.09	O1-C17-O2	107.6	O7-C20-C19	121	C14-C16-H37	109.4	H47-C28-C32	119.6
O3-H41	0.964	C19-C21	1.462	O1-C17-C15	108.7	O7-C20-C24	111.5	C17-C15-H36	107.6	C28-C32-C33	120.3
O4-C14	1.42	C19-C20	1.367	O1-C17-H38	111.3	O8-C21-C19	122.3	C15-C17-H38	111.1	C28-C32-H49	119.9
O4-H42	0.965	C20-C24	1.473	C17-O2-C19	119	O8-C21-C22	122.3	C18-C16-H37	108.6	C30-C29-H48	120.2
O5-C15	1.424	C21-C22	1.448	O2-C17-C15	108.1	C21-O8-H50	100.3	C16-C18-H39	108.9	C31-C33-C32	120.1
O5-H43	0.965	C22-C23	1.4	O2-C17-H38	110	H50-O9-C25	107.4	C16-C18-H40	109.6	C33-C32-H49	119.8
O6-C18	1.418	C22-C25	1.427	O2-C19-C21	120.3	O9-H50-O8	147.8	H39-C18-H40	108.6		
O6-H44	0.967	C23-C26	1.389	O2-C19-C20	118.5	O9-C25-C22	120.6	C21-C19-C20	121.1		
O7-C23	1.364	C24-C28	1.403	C13-O3-H41	107.7	O9-C25-C29	119.4	C19-C21-C22	115.3		
O7-C20	1.364	C24-C27	1.406	O3-C13-C14	107.4	C30-O10-H51	110.2	C19-C20-C24	127.5		
O8-C21	1.246	C25-C29	1.388	O3-C13-C15	111.8	O10-C30-C26	121.7	C20-C24-C28	122.2		
O9-H50	0.989	C26-C30	1.397	O3-C13-H34	109.5	O10-C30-C29	116.5	C20-C24-C27	118.8		
O9-C25	1.338	C26-H45	1.083	C13-O3-H42	107.4	C31-O11-H52	108.8	C21-C22-C23	120.4		
O10-C30	1.36	C27-H46	1.081	H41-O3-H42	111.1	O11-C31-C27	119.6	C21-C22-C25	121.6		
O10-H51	0.963	C27-C31	1.385	C14-O4-H42	108.6	O11-C31-C33	120.8	C23-C22-C25	118		
O11-C31	1.36	C28-H47	1.08	O4-C14-C13	110.4	O11-H52-O12	112.5	C22-C23-C26	122.7		
O11-H52	0.966	C28-C32	1.393	O4-C14-C16	108.6	C33-O12-H53	111	C22-C25-C29	120.1		
O12-C33	1.371	C29-C30	1.397	O4-C14-H35	107	O12-C33-C31	115.2	C23-C26-C30	117.7		
O12-H53	0.963	C29-H48	1.082	O4-H42-O3	110.8	O12-C33-C32	124.7	C23-C26-H45	120.1		
C13-C14	1.528	C31-C33	1.404	C15-O5-H43	112.7	C33-O12-H52	82.7	C28-C24-C27	119		
C13-C15	1.527	C32-C33	1.389	O5-C15-C13	107.5	H53-O12-H52	166.3	C24-C28-H47	120.2		
C13-H34	1.1	C32-H49	1.086	O5-C15-C17	111	C14-C13-C15	111.4	C24-C28-C32	120.1		
C14-C16	1.531	O8-H50	1.719	O5-C15-H36	111.2	C14-C13-H34	108.2	C24-C27-H46	120.9		
C14-H35	1.099	O12-H52	2.161	C18-O6-H44	112.9	C13-C14-C16	109.2	C24-C27-C31	120.8		
C15-C17	1.097			O6-C18-C16	108.7	C13-C14-H35	108.5	C25-C29-C30	119.7		
C15-H36	1.534			O6-C18-H39	105.6	C15-C13-H34	108.4	C25-C29-H48	120.1		

3. Results and Discussion

3.1 Molecular Geometric Parameters

"The DFT calculation in the B3LYP/6311++G(d,p) level was used to optimize the molecular geometry of the compound 5H1P1C4O1G and the structural parameters (bond lengths and bond angles) are all found to be in excellent agreement with anticipated values of analogous organic systems [13]."

The C-C bond lengths of the aromatic and conjugated structure are mainly in the range of 1.38-1.40 Åwhich demonstrates that the pi-electrons are highly delocalized in the system of the rings. Conversely, the aliphatic C-C bonds (ex: C13-C14 and C14-C16) are slightly longer at approximately 1.52-1.53 Å, which is characteristic of single bonds. The lengths of the C-O bonds also depend on the chemical environment of those bonds: the carbonyl group (C=O) is shorter (~1.24 Å), which, of course, is the indication of a presence of the double bond, but the C-O single bonds range between 1.33 and 1.44 Å. The OH bond lengths are seen to be at 0.96- 0.98 Å characteristic of hydroxyl groups [14].

The molecular conformation is further supported by the bond angles. The bond angles around the sp2 hybridized carbon atoms are similar to trigonal planar geometry, e.g. 120o, as the aromatic and carbonyl containing regions (e.g. C-C-C and O-C-C angles). Conversely, the bond angles of the sp3 hybridized centers were found to be close to 109o, a tetrahedral geometry especially in the aliphatic chain segments. C-O-H and O-C-O angles are changed between 100 and 120o, depending on hydrogen bonding and steric interactions [15].

It is worth noting that there are slight differences in bond lengths and angles which can be attributed to intramolecular hydrogen bonding, delocalization of electrons, and substituent effects in the molecule. All in all, the optimized geometry supports the stable structure of a mixture of planar aromatic region and non-planar aliphatic segments, which leads to the structural flexibility and reactivity of the molecule [16].

3.2. FT-IR and FT-Raman Vibrational Analysis of 5H1P1C4O1G

The FT-IR spectrum of 5H1P1C4O1G was measured in 4000-500 cm -1 with a PerkinElmer spectrophotometer, and FT-Raman spectrum in 3500-500 cm -1 with a Bruker RFS Raman spectrometer. DFT was used to compute the theoretical vibrational frequencies with the B3LYP/6-311++G(d,p) level with scaling factor of 0.961 to address anharmonicity and the basis set limitations [17].

Being a nonlinear molecule, 5H1P1C4O1G has (3N-6) normal vibrational modes. The PED analysis was done on VEDA4 program to perform vibrational assignments. Table 2 shows the experimental and scaled theoretical frequencies and PED contribution giving good agreement with the simulated spectra (Figure 2).

It is suggested that minor differences in experimental and theoretical values are caused by solid-state effects, intermolecular interactions, temperature differences, and limitations of the instruments.

Table 2. Experimental and scaled DFT vibrational wavenumbers (cm^{-1}), IR and Raman intensities, and PED assignments of 5H1P1C4O1G (B3LYP/6-311++G(d,p))

Vibrational Modes	Experimental Frequency (cm^{-1})		Frequency (cm^{-1})		Infrared intensity		Raman intensity		PED Contribution (%)
	FT-IR	FT-RAMAN	Unscaled	Scaled	Relative	Absolute	Relative	Absolute	
153	3350	3425	3843.48	3693.58	139.1745	4.06	4.06	234.5792	νOH (100)
152	3325	3380	3831.33	3681.91	91.2763	12.22	12.24	151.8514	νOH (100)
151	3300	3320	3818.37	3669.45	49.1346	32.26	32.3	69.7792	νOH (100)
150	3250	3210	3810.8	3662.18	57.2553	26.76	26.79	94.7829	νOH (98)
149	3200	3082	3794.58	3646.59	108.2784	8.26	8.27	159.9507	νOH (99)
148	3085	2935	3791.44	3643.57	172.4508	1.89	1.89	133.8535	νOH (98)

147	3055	2865	3777.16	3629.85	103.3906	9.25	9.26	97.3415	νOH (98)
146	3020	1662	3316.9	3187.54	459.1987	0	0	147.8054	νOH (99)
145	2950	1655	3233.28	3107.18	1.5399	96.52	96.63	34.1964	νCH (99)
144	2935	1610	3215.67	3090.26	1.2073	97.26	97.37	46.0984	νCH (100)
143	2925	1582	3215.4	3090	0.1636	99.62	99.74	174.6619	νCH (99)
142	2875	1462	3190.23	3065.81	1.6627	96.24	96.36	80.5645	νCH (100)
141	2860	1270	3161.27	3037.98	12.6227	74.78	74.87	126.2581	νCH (99)
140	2850	1220	3112.13	2990.76	13.8632	72.67	72.76	114.3156	νCH (79)
139	1660	1172	3032.26	2914	64.0636	22.88	22.9	3.934	νCH (88)
138	1645	1115	3015.88	2898.26	2.1732	95.12	95.23	95.144	νCH (88)
137	1630	1088	3008.6	2891.26	56.496	27.23	27.26	7.2183	νCH (89)
136	1580	1058	2993.02	2876.29	1.342	96.96	97.07	1.0879	νCH (46)
135	1490	1012	2986.98	2870.49	2.5121	94.38	94.49	220.6508	νCH (46)
134	1465	855	2983.8	2867.43	28.3986	52	52.06	41.6787	νCH (46)
133	1455	835	1687.04	1621.25	594.8158	0	0	280.6262	νCC + βHOC
132	1445	778	1653.51	1589.02	6.3598	86.38	86.48	431.6091	νCC
131	1260	765	1636.67	1572.84	198.711	1.03	1.03	285.5346	νCC
130	1210	702	1634.9	1571.14	351.0027	0.03	0.03	33.8835	νCC + νOC
129	1175	615	1623.63	1560.31	191.4877	1.22	1.22	118.0892	νCC (14)
128	1160	590	1606.99	1544.32	77.6933	16.71	16.73	1045.773	νCC (40)
127	1150	545	1545.94	1485.65	158.5759	2.6	2.6	27.327	βHCC (19)
126	1120	520	1523.91	1464.48	235.54	0.44	0.44	160.0294	νCC + βHCC
125	1110	495	1502.29	1443.7	0.9358	97.87	97.98	8.0992	νCC + βHCH
124	1100	470	1490.15	1432.03	176.8721	1.7	1.71	13.642	νOC + βHCC
123	1090	445	1481.76	1423.97	1.6508	96.27	96.38	3.8757	νOC
122	1080	420	1449.91	1393.36	68.0371	20.88	20.9	122.076	νCC
121	1070	395	1440.34	1384.17	12.8639	74.36	74.45	6.561	νCC + τHCCC
120	1050	370	1433.52	1377.61	17.9617	66.13	66.21	8.1139	νCC

119	1015	345	1427.79	1372.11	38.0308	41.66	41.71	30.9899	βHCO
118	1008	320	1424.06	1368.52	101.224	9.72	9.73	344.2253	βHCO
117	1000	295	1416.3	1361.06	31.188	48.77	48.82	6.9273	βHCO
116	860	270	1412.79	1357.69	6.9927	85.13	85.23	2.3714	βHCO + ωCCCH
115	845	245	1394.54	1340.15	7.365	84.4	84.5	6.582	βHCO + τHCOC
114	830	220	1383.77	1329.8	327.8134	0.05	0.05	326.465	νCC
113	780	195	1371.37	1317.89	10.0902	79.27	79.36	2.3291	βHOC + τHCOC
112	770	170	1368.18	1314.82	31.6164	48.29	48.34	28.1402	βHCO
111	760	145	1362.49	1309.35	10.8997	77.8	77.9	2.2912	βHCO
110	705	120	1349.61	1296.98	35.4419	44.22	44.27	1.3257	βHCO
109	690	95	1343.77	1291.36	25.849	55.15	55.21	52.792	βHCO
108	670	70	1336.48	1284.36	274.2596	0.18	0.18	64.0146	βHCO
107	650	<50	1335.35	1283.27	45.4668	35.1	35.14	7.7351	βHCO
106	620	—	1317.42	1266.04	30.0798	50.03	50.09	2.8081	βHCO
105	600	—	1313.45	1262.23	180.8468	1.55	1.56	133.6031	νOC
104	580	—	1287.85	1237.62	123.8311	5.78	5.78	21.9316	νOC
103	560	—	1283.69	1233.63	44.7947	35.65	35.69	1.1498	νOC
102	540	—	1264.13	1214.83	61.0552	24.52	24.54	2.3886	βHOC
101	<520	—	1255.51	1206.55	26.1502	54.76	54.83	1.9029	βHOC
100	—	—	1242.47	1194.01	99.5185	10.11	10.12	5.5136	βHOC
99	—	—	1240.38	1192.01	167.5842	2.11	2.11	11.2588	βHOC
98	—	—	1232.48	1184.41	19.0318	64.52	64.59	0.5172	βHOC
97	—	—	1222.81	1175.12	312.5793	0.07	0.07	4.7404	νOC
96	—	—	1215.06	1167.67	85.6545	13.91	13.93	34.1696	νOC
95	—	—	1203.96	1157.01	35.6306	44.02	44.08	0.4464	νOC
94	—	—	1196.55	1149.88	14.2927	71.96	72.04	1.2762	νOC
93	—	—	1176.73	1130.84	29.7218	50.44	50.5	2.4034	βHOC
92	—	—	1172.86	1127.12	225.5447	0.56	0.56	1.092	βHOC

91	—	—	1157.52	1112.38	37.187	42.47	42.53	3.2728	βHOC
90	—	—	1143.51	1098.91	23.9486	57.61	57.68	3.9881	βHOC
89	—	—	1129.18	1085.14	145.7093	3.49	3.49	4.7835	νOC
88	—	—	1126.72	1082.78	78.3754	16.45	16.47	17.1977	νOC
87	—	—	1110.27	1066.97	71.5254	19.26	19.29	7.1472	νOC
86	—	—	1108.71	1065.47	74.5152	17.98	18	1.6612	νOC
85	—	—	1099.84	1056.95	124.6168	5.67	5.68	0.757	νCC
84	—	—	1094.27	1051.59	258.5253	0.26	0.26	14.1231	νCC
83	—	—	1085.52	1043.18	14.1776	72.15	72.23	3.4608	βCCC
82	—	—	1078.08	1036.03	166.8777	2.14	2.15	7.6985	βCCC
81	—	—	1067.01	1025.4	34.5469	45.14	45.19	1.2193	βCCC
80	—	—	1052.65	1011.6	179.3609	1.61	1.61	5.7354	νOC
79	—	—	1040.51	999.93	89.5956	12.71	12.72	11.4527	νOC
78	—	—	1022.78	982.89	29.4713	50.73	50.79	1.3752	νCC
77	—	—	1006.86	967.59	30.3985	49.66	49.72	5.5321	νCC
76	—	—	1000.41	961.39	17.1896	67.31	67.39	11.5254	τHCCC
75	—	—	987.79	949.27	111.3778	7.7	7.7	1.7053	τHCCC
74	—	—	951.75	914.63	1.9006	95.72	95.83	2.5903	νCC
73	—	—	947.05	910.12	23.6388	58.02	58.09	23.0461	τHCCC
72	—	—	901.88	866.71	19.4966	63.83	63.91	4.0415	τCCCO
71	—	—	893.85	858.99	35.5392	44.12	44.17	3.8784	τCCCO
70	—	—	858.73	825.24	0.4204	99.04	99.15	0.1908	τHOCC
69	—	—	855.45	822.09	4.8562	89.42	89.53	11.2588	τHOCC
68	—	—	834.59	802.04	106.8803	8.53	8.54	0.5172	ωOCCC
67	—	—	821.16	789.13	31.7737	48.11	48.17	4.7404	ωOCCC
66	—	—	795.85	764.81	44.213	36.13	36.17	34.1696	νCC
65	—	—	792.3	761.4	32.8178	46.97	47.03	0.4464	ωOCCC
64	—	—	784.53	753.93	8.9261	81.42	81.52	1.2762	ωOCCC
63	—	—	739.35	710.52	4.721	89.7	89.81	2.4034	ωOCCC
62	—	—	725.04	696.76	2.5453	94.31	94.42	1.092	τCCCC
61	—	—	709.86	682.18	8.0146	83.15	83.25	3.2728	βCCO
60	—	—	691.35	664.39	2.4637	94.49	94.6	3.9881	ωOCCC
59	—	—	677.11	650.7	2.7561	93.85	93.96	4.7835	τCCOC
58	—	—	662.61	636.77	17.4717	66.88	66.96	17.1977	βCCC
57	—	—	639.17	614.24	3.8201	91.58	91.69	7.1472	ωOCCC
56	—	—	636.51	611.69	15.0449	70.72	70.81	1.6612	βCCC

55	—	—	616.96	592.9	1.8943	95.73	95.85	0.757	βCCC
54	—	—	612.25	588.37	6.0184	87.06	87.16	14.1231	βCCC
53	—	—	606.11	582.47	13.2363	73.73	73.82	3.4608	βCCC
52	—	—	604.66	581.08	51.0737	30.85	30.89	7.6985	βCCC
51	—	—	596.31	573.05	18.9486	64.64	64.72	1.2193	βCCC
50	—	—	577.71	555.18	12.5207	74.95	75.04	5.7354	βCCC
49	—	—	572.77	550.43	3.1355	93.03	93.15	11.4527	βCCC
48	—	—	567.06	544.94	14.4212	71.74	71.83	1.3752	βCCC
47	—	—	524.64	504.18	9.4973	80.36	80.45	5.5321	βOCC
46	—	—	504.97	485.28	4.4375	90.29	90.39	11.5254	βOCC
45	—	—	496.04	476.69	2.035	95.42	95.54	3.6885	βCOC
44	—	—	478.55	459.89	135.0404	4.46	4.47	8.4865	βOCC
43	—	—	466.87	448.66	33.5509	46.18	46.24	1.2663	βCCC + βOCC
42	—	—	456.06	438.27	18.4636	65.37	65.45	2.5207	τHOCC
41	—	—	455.03	437.28	4.609	89.93	90.04	3.1957	τHOCC
40	—	—	427.08	410.42	4.0212	91.16	91.26	3.693	τHOCC
39	—	—	422.95	406.45	49.6951	31.85	31.88	1.9445	τHOCC
38	—	—	416.54	400.29	75.363	17.63	17.66	2.5032	τHOCC
37	—	—	411.12	395.09	54.5607	28.47	28.5	0.8548	τHOCC
36	—	—	402.75	387.04	32.7272	47.07	47.12	11.018	τHOCC
35	—	—	394.88	379.48	47.0198	33.87	33.91	1.3892	τHOCC
34	—	—	391.35	376.09	59.3183	25.52	25.55	5.9913	τHOCC
33	—	—	380.94	366.08	42.5549	37.54	37.58	2.8243	ωOCCC
32	—	—	372.49	357.96	0.4834	98.89	99.01	2.2682	βCCC + βOCC
31	—	—	351.35	337.65	24.5447	56.83	56.89	1.4469	τHOCC
30	—	—	346.15	332.65	98.6404	10.32	10.33	2.1955	τHOCC
29	—	—	334.4	321.36	7.693	83.77	83.87	1.5506	τHOCC
28	—	—	328.27	315.47	5.7526	87.59	87.7	0.686	τHOCC
27	—	—	310.75	298.63	6.8447	85.42	85.52	0.5816	βOCC
26	—	—	302.41	290.62	3.1901	92.92	93.03	1.1623	βOCC
25	—	—	290.6	279.27	10.6229	78.3	78.39	2.3858	ωCCCC
24	—	—	267.8	257.36	11.2058	77.26	77.35	1.42	βOCC
23	—	—	260.26	250.11	4.7608	89.62	89.72	0.9127	βOCC
22	—	—	249.49	239.76	7.6839	83.78	83.88	1.1204	τCCCO
21	—	—	245	235.44	36.3374	43.31	43.37	1.1792	βCCC + τHOCC
20	—	—	236.47	227.25	15.8196	69.47	69.55	0.571	νCC
19	—	—	229.24	220.3	62.7429	23.58	23.61	1.7031	νCC
18	—	—	227.31	218.44	26.698	54.08	54.14	0.8649	νCC
17	—	—	222.26	213.59	12.3201	75.3	75.39	3.1477	τCCCC
16	—	—	200.35	192.54	3.1169	93.07	93.18	5.3793	τCCCC

15	—	—	196.54	188.87	3.8135	91.59	91.7	0.9854	βCCO
14	—	—	172.19	165.47	1.1395	97.41	97.53	0.953	βOCO
13	—	—	138.91	133.49	1.8925	95.74	95.85	0.4757	ωCCOC
12	—	—	137.93	132.55	0.7871	98.2	98.32	1.0053	βOCC
11	—	—	117.31	112.73	0.633	98.55	98.67	0.0817	τOCCC
10	—	—	111.73	107.37	1.6381	96.3	96.41	0.2666	τCOCC
9	—	—	103.41	99.38	1.2473	97.17	97.28	0.348	βOCC
8	—	—	87.4	83.99	0.9526	97.83	97.95	1.176	βOCC
7	—	—	64.47	61.96	0.924	97.89	98.01	2.3538	βOCC
6	—	—	58.29	56.02	0.6664	98.48	98.59	1.3684	βOCC
5	—	—	41.44	39.82	0.467	98.93	99.05	1.4195	τCOCC
4	—	—	36.3	34.88	1.177	97.33	97.44	3.7115	τCOCC
3	—	—	26.71	25.67	0.4554	98.96	99.07	2.9331	τCOCC
2	—	—	19.42	18.66	0.0515	99.88	100	3.1773	τCOCC
1	—	—	13.44	12.92	0.313	99.28	99.4	0.5832	τOCOC

FT-IR and FT-Raman spectra were used to obtain the vibrational spectral analysis of 5H1P1C4O1G, and the frequencies of the bands were determined by DFT calculations and PED contributions to identify bands correctly [18]. High-frequency region (3350-3000 cm -1) OH stretching vibrations (νOH) with mode 153-146 with about 100 percent PED contribution are observed, which confirms the pure nature of the stretching bands. The experimental bands observed at 3350-3020 cm -1 (FT-IR) and the related Raman shifts show that there were strong interactions in terms of hydrogen bonding, and are also confirmed by the fact that scaled and unscaled frequencies differ slightly [19].

The C-H stretching bands (CH) are found at 2950-2850 cm -1 (modes 145-140) with PED values of 79-100, which validates their predominantly stretching nature. These bands are provided with the presence of aliphatic C-H groups and moderate Raman activity with a high intensity of IR that shows alterations of the dipole moment during the vibration [21].

"The vibrational modes in the mid-frequency range (1700 -1000 cm -1) can mainly be related to C -C stretching (νCC), C -O stretching (νOC) and other bending vibrations including βHCO, βHB. The observation of a powerful Raman-active mode at 1544 cm -1 (mode 128) with the highest intensity indicates the presence of skeletal C-C stretching vibrations, which confirms the presence of a conjugated structure. The C-O stretching vibrations are attributed to the existence of oxygen-containing functional groups, the bands of which are mostly located in the region 1200-1000 cm-1. The PED analysis indicates a mixed contribution in this region indicating that the stretching and bending vibrations are coupled to each other [22]."

In-plane and out-of-plane bending vibrations are dominant in the fingerprint region (1000-400 cm -1), and this region contains β-CCC, βOCC and torsional modes (τ). The Raman activity of these modes is moderate to strong which is an indication of the structural rigidity and stability of the molecular framework. The low-frequency range below 400 cm -1 is composed primarily of torsional and skeletal deformation vibrations e.g. τCCCC, τHOCC, and τCOCC, which are linked to collective molecular motions and validate the skeletal flexibility of the molecular structure.

Overall, the calculated vibrational frequencies show good agreement with the experimental FT-IR and FT-Raman data, validating the computational methodology. The PED analysis provides reliable mode assignments, indicating minimal mode mixing in the high-frequency region and well-defined vibrational characteristics throughout the spectrum. The presence of strong hydrogen bonding, conjugated C–C framework, and oxygen functional groups is clearly evidenced from the spectral analysis.

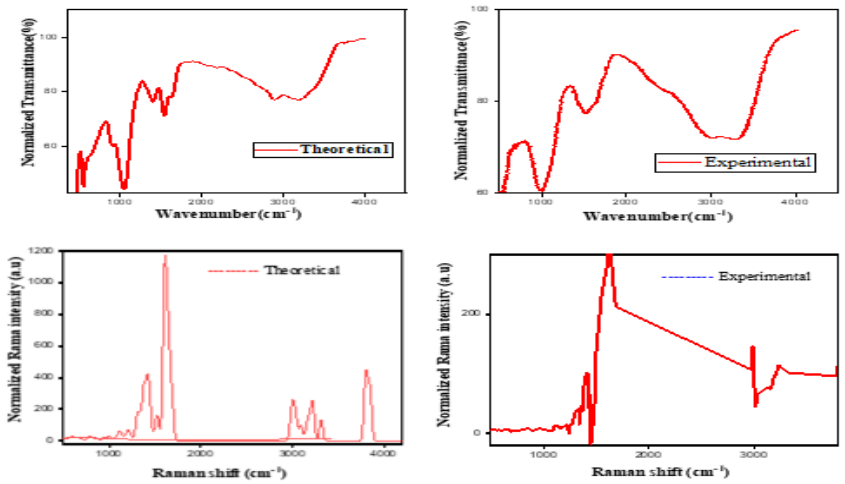

Fig. 2. FT-IR and FT-Raman spectral analysis of 5H1P1C4O1G.

3.3. HOMO–LUMO Analysis of Frontier Molecular Orbitals

"The most important in interpreting the electronic structure and reactivity of a molecule are frontier molecular orbitals, especially the highest occupied (HOMO) orbital and the lowest unoccupied (LUMO) orbital [23]. The difference in energy of these orbitals provides information on stability, chemical behaviour, and other properties, including hardness, softness, and polarizability [24]. These aspects also play a major role in learning the nature of charge transfer and potential biological activity [25]."

Table 3. Quantum Chemical Reactivity Parameters and Stability Profile of 5H1P1C4O1G in Different Media

Electronic Descriptor	Gas Phase	Methanol	Ethanol	DMSO
Energy of HOMO (eV)	-6.411	-6.274	-6.629	-6.271
Energy of LUMO (eV)	-2.396	-2.285	-2.286	-2.284
Vertical Ionization Potential (eV)	6.411	6.274	6.629	6.271
Electron Affinity Energy (eV)	2.396	2.285	2.286	2.284
Frontier Orbital Energy Gap (eV)	4.015	3.989	4.343	3.987
Mulliken Electronegativity (χ)	4.404	4.280	4.458	4.278
Electronic Chemical Potential (μ)	-4.404	-4.280	-4.458	-4.278
Global Hardness (η)	2.008	1.995	2.172	1.994
Global Softness (S)	0.249	0.251	0.230	0.251
Global Electrophilicity Index (ω)	4.830	4.591	4.575	4.589
Fractional Electron Transfer (ΔN)	2.194	2.146	2.053	2.146
Electron Donating Capability (ω^-)	7.282	6.980	7.075	6.977
Electron Accepting Capability (ω^+)	2.879	2.701	2.618	2.700

The HOMO and LUMO energies of the compound 5H1P1C4O1G in the gas phase are determined as -6.411 eV and -2.396 eV respectively, with an energy gap of 4.015 eV, and this means that the compound is moderate in stability with a moderate reactivity [26]. The HOMO levels are slightly enhanced in the polar solvents (methanol, ethanol and DMSO) with the LUMO virtually unchanged at -2.284 eV, so the energy gap is less (approximately 3.98–3.99 eV). Such a decrease indicates greater delocalization of electrons and chemical reactivity in solution as presented in Table 3 [27].

The reduced HOMO LUMO gap in solvent media allows electronic excitation and efficient intramolecular charge transfer that is useful in nonlinear optical behaviour [28]. The gap values that lie below 5 eV also suggest favourable redox reactions and possible biological interactions [29].

The consideration of solvent effects by the IEFPCM model reveals that the orbital energies differ slightly, suggesting that the fundamental electronic structure of 5H1P1C4O1G remains mostly intact as presented in Fig 3 [30]. The HOMO is primarily concentrated on parts of the molecule that are rich in

electrons, with the LUMO being concentrated on the parts of the molecule that lack electrons, which is a confirmation of the effective separation of charge. A similarity in the orbital distribution of all media indicates that the solvent has a minimal effect on the electron density distribution [31].

The ionization potential is lower in the solution, at approximately 6.27 eV compared to 6.411 eV in the gas phase, and therefore the electron in the solution is easier to remove, whereas the electron affinity is slightly lower (~2.284 eV), which is indicative of stabilization of the accepting orbital. Electrophilicity index is always high and shows a high electron-accepting power [32]. Reduction in chemical hardness and increase in softness in solvent media are additional supporting factors towards enhanced reactivity and polarizability [33]. In general, the findings show that 5H1P1C4O1G has stable electronic properties with enhanced reactivity in polar conditions, and it could be a promising candidate in charge transfer and other applications[34].

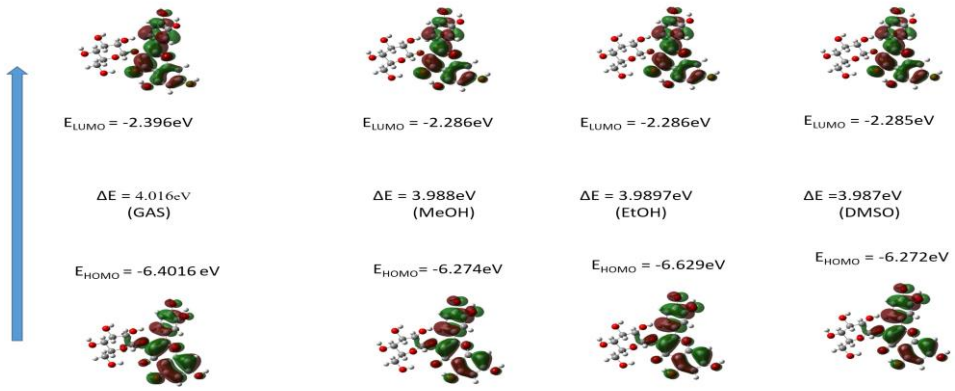

Fig. 3. Variation of HOMO and LUMO energy levels of 5H1P1C4O1G in different solvent media.

3.4 Charge Distribution Analysis Using Molecular Electrostatic Potential (MEP)

The molecular electrostatic potential (MEP) surface of 5H1P1C4O1G gives a good display of the charge distribution and interaction behaviour of the molecule. Negative potentials in the form of regions are primarily found around the oxygen atom within the hydroxyl and carbonyl groups, which points to the electron-rich sites. These regions are, however, limited and not extended over the molecular structure, although the aromatic backbone has mostly neutral to slightly positive potential, which corresponds to the nonpolar character as a whole [35].

The localization of the negative potential restricts strong interactions with polar environments, even though the molecule has electronegative oxygen atoms that can form hydrogen bonds. This means that there should be only moderate solute-solvent interactions. The fact that MEP surfaces in the gas phase, in methanol and in DMSO, indicate that the overall charge distribution is largely unchanged indicates that the solvent medium does not fundamentally change the intrinsic electronic structure.

The MEP surfaces in the gas phase, methanol, and DMSO reveal that the overall charge distribution remains largely unchanged across different environments, indicating that the intrinsic electronic structure is preserved. The electrostatic potential in the gas phase ranges from -8.535×10^{-2} to $+8.535 \times 10^{-2}$ a.u., whereas in DMSO it extends from −0.103 to +0.103 a.u., showing a slight increase in polarization due to solvent effects. A similar trend is observed in methanol, reflecting moderate stabilization of charge-separated regions.

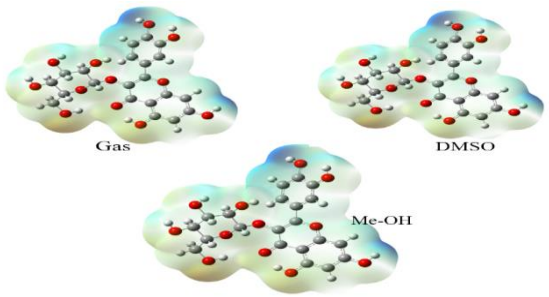

Fig.4 Molecular electrostatic potential of 5H3M1P1C4O for different solvents

Overall, the MEP analysis reveals that 5H1P1C4O1G possesses localized polar regions within a predominantly nonpolar framework, leading to moderate solvent interaction and solvent-independent electronic distribution.

Table 4. Evaluation of Fock Matrix Stabilization Energies Using Second-Order Perturbation Theory in 5H1P1C4O1G

Donor Orbital Energy (Ed/e)	Orbital type	Donor orbital	Donor Orbital Energy (Ed/e)	Orbital type	Acceptor orbital	Second-Order Stabilization Energy E(2)[a] Kcal/mol a.u	Energy Gap ΔE = E(j)-E(i)[b] a.u	Fock Matrix ElementF(i,j)[c] a.u.
1.98855	σ	O 12 - H 53	0.39715	π*	C 32 - C 33	15973.2	0.04	0.748
0.39715	π*	C 32 - C 33	0.0364	σ*	C 16 - H 37	4193.25	0.04	0.744
1.97751	σ	C 32 - C 33	0.04343	σ*	C 17 - H 38	3759.81	0.07	0.476
1.9715	σ	C 31 - C 33	0.04343	σ*	C 17 - H 38	3496.33	0.07	0.429
1.97293	σ	C 28 - C 32	0.04343	σ*	C 17 - H 38	2622.78	0.04	0.308
1.98686	σ	O 11 - H 52	0.04343	σ*	C 17 - H 38	1706.99	0.05	0.253
1.97657	LP1	O12	0.02011	σ*	C 27 - C 31	1629.89	0.22	0.532
1.99405	σ	O 12 - C 33	0.39715	π*	C 32 - C 33	1350.92	0.67	0.949
1.99405	σ	O 12 - C 33	0.02011	σ*	C 27 - C 31	1143.69	0.43	0.63
1.97241	σ	C 27 - C 31	0.04343	σ*	C 17 - H 38	985.85	0.05	0.197
1.97657	LP1	O12	0.39715	π*	C 32 - C 33	970.86	0.46	0.661
1.99405	σ	O 12 - C 33	0.04343	σ*	C 17 - H 38	926.67	0.21	0.402
1.96891	σ	C 24 - C 28	0.04343	σ*	C 17 - H 38	779.89	0.03	0.141
1.96449	σ	C 24 - C 27	0.04343	σ*	C 17 - H 38	466.1	0.03	0.103
1.98855	σ	O 12 - H 53	0.0364	σ*	C 16 - H 37	435.98	0.07	0.158
1.99325	σ	O 11 - C 31	0.04343	σ*	C 17 - H 38	375.52	0.26	0.279
0.39715	π*	C 32 - C 33	0.02953	σ*	C 16 - C 18	311.26	0.27	0.556
1.98686	σ	O 11 - H 52	0.01236	σ*	C 27 - H 46	308.81	3.63	0.946
1.99405	σ	O 12 - C 33	0.0364	σ*	C 16 - H 37	265.31	0.71	0.39
1.97657	LP1	O12	0.0364	σ*	C 16 - H 37	261.82	0.49	0.322
1.99325	σ	O 11 - C 31	0.01236	σ*	C 27 - H 46	237.56	3.84	0.854
1.97751	σ	C 32 - C 33	0.0364	σ*	C 16 - H 37	216.98	0.57	0.315
0.36447	π*	O 8 - C 21	0.26731	π*	C 19 - C 20	194.78	0.01	0.077
0.47075	π*	C 22 - C 23	0.34972	π*	C 25 - C 29	181.22	0.02	0.078
0.39715	π*	C 32 - C 33	0.41912	π*	C 26 - C 30	166.6	0.2	0.254
0.41912	π*	C 26 - C 30	0.47075	π*	C 22 - C 23	165.16	0.02	0.081
1.97782	LP1	O11	0.01236	σ*	C 27 - H 46	157.04	3.53	0.667
1.97766	σ	C 32 - H 49	0.0364	σ*	C 16 - H 37	154.22	0.37	0.213
1.9715	σ	C 31 - C 33	0.0364	σ*	C 16 - H 37	144.72	0.56	0.255
0.35406	π*	C 27 - C 31	0.40787	π*	C 24 - C 28	142.83	0.02	0.079
1.97751	σ	C 32 - C 33	0.02011	σ*	C 27 - C 31	134.84	0.29	0.177
1.99405	σ	O 12 - C 33	0.02953	σ*	C 16 - C 18	112.07	0.94	0.291
1.96843	σ	C 20 - C 24	0.04343	σ*	C 17 - H 38	102.47	0.01	0.029
1.97657	LP1	O12	0.02953	σ*	C 16 - C 18	102.06	0.72	0.243
1.97751	σ	C 32 - C 33	0.02953	σ*	C 16 - C 18	96.51	0.8	0.248
1.97766	σ	C 32 - H 49	0.02011	σ*	C 27 - C 31	96.28	0.09	0.082
1.6625	π	C 27 - C 31	0.39715	π*	C 32 - C 33	93.57	0.06	0.068
0.41912	π*	C 26 - C 30	0.34972	π*	C 25 - C 29	78.94	0.04	0.08
1.88569	LP2	O12	0.39715	π*	C 32 - C 33	78.77	0.14	0.102
1.9715	σ	C 31 - C 33	0.02953	σ*	C 16 - C 18	67.43	0.79	0.206
1.66598	π	C 24 - C 28	0.39715	π*	C 32 - C 33	66.3	0.05	0.054
1.9715	σ	C 31 - C 33	0.02011	σ*	C 27 - C 31	63.77	0.28	0.12
1.95458	LP1	O2	0.02011	σ*	C 27 - C 31	62.59	0.09	0.068

1.98686	σ	O 11 - H 52	0.02011	σ*	C 27 - C 31	61.6	0.26	0.114
1.97766	σ	C 32 - H 49	0.02953	σ*	C 16 - C 18	60.88	0.6	0.17
0.39715	π*	C 32 - C 33	0.35406	π*	C 27 - C 31	59.14	0.21	0.161
1.97293	σ	C 28 - C 32	0.0364	σ*	C 16 - H 37	57.99	0.54	0.158
1.98855	σ	O 12 - H 53	0.02953	σ*	C 16 - C 18	54.69	0.3	0.115
1.98686	σ	O 11 - H 52	0.0364	σ*	C 16 - H 37	50.29	0.54	0.148
1.97869	LP1	O4	0.01689	σ*	C 18 - H 40	0.57	0.99	0.021
0.36447	π*	O 8 - C 21	0.34972	π*	C 25 - C 29	0.57	0.03	0.006
0.35406	π*	C 27 - C 31	0.01689	σ*	C 18 - H 40	0.57	0.39	0.031
0.41912	π*	C 26 - C 30	0.00902	σ*	O 11 - H 52	0.56	0.39	0.029
0.39715	π*	C 32 - C 33	0.36447	π*	O 8 - C 21	0.56	0.21	0.016
1.98725	σ	O2-C19	0.0668	σ*	C 19 - C 21	0.54	1.34	0.024
1.98855	σ	O 12 - H 53	0.03027	σ*	O 7 - C 23	0.54	0.58	0.016
1.66598	π	C 24 - C 28	0.00835	σ*	O 5 - H 43	0.54	0.7	0.019
1.98512	σ	O 9 - H 50	0.03466	σ*	C 22 - C 25	0.53	1.24	0.023
1.97577	σ	C 16 - H 37	0.03158	σ*	O 1 - C 16	0.53	0.79	0.018
1.97002	σ	C 23 - C 26	0.03027	σ*	O 7 - C 23	0.53	1.06	0.021
1.97293	σ	C 28 - C 32	0.02177	σ*	O 10 - C 30	0.53	1.06	0.021
1.95458	LP1	O2	0.02154	σ*	C 29 - C 30	0.53	3.08	0.036
1.99112	σ	O5-C15	0.04343	σ*	C 17 - H 38	0.52	0.16	0.008
1.97657	LP1	O12	0.03818	σ*	C 13 - H 34	0.52	1.05	0.021
1.9715	σ	C 31 - C 33	0.02305	σ*	O 12 - C 33	0.51	1.05	0.021
1.95518	LP1	O1	0.01689	σ*	C 18 - H 40	0.51	0.95	0.02
0.35406	π*	C 27 - C 31	0.01236	σ*	C 27 - H 46	0.51	2.92	0.081
1.9937	σ	O 9 - C 25	0.02154	σ*	C 29 - C 30	0.5	3.46	0.037
1.98855	σ	O 12 - H 53	0.02305	σ*	O 12 - C 33	0.5	0.57	0.015
1.97751	σ	C 32 - C 33	0.02305	σ*	O 12 - C 33	0.5	1.06	0.021
1.95458	LP1	O2	0.01142	σ*	O 8 - C 21	0.5	1.07	0.021

Table 5. NBO Hybrid Orbital Composition and Electron Density Distribution of Selected Lewis Orbitals in 5H1P1C4O1G

	EDA% / EDB%	**NBO hybrid / orbitals**	**s,p %**	
σ (O12-C33) / 1.99405	66.96 / 33.04	0.8183(sp1.91) O12 0.5748(sp3.11)C33	34.28, 65.64	24.29, 75.49
σ (C20-C24) / 1.96843	50.18 / 49.82	0.7084(sp1.75) C20/ 0.7058(sp2.25)C24	36.29, 63.68	30.80, 69.15
σ (C32-H49) / 1.97766	60.52 / 39.48	0.7779(sp2.48)C32/ 0.6283(sp)H49	28.72, 71.24	99.95, 0.05
σ (O11-H52) / 1.98686	74.76 / 25.24	0.8647(sp3.65) O11/ 0.5023(sp)C33	21.48, 78.42	99.85, 0.15
LP1 (O12) / 1.97657		(sp1.28)	43.92, 56.04	

3.5. Natural Bond Orbital Analysis of 5H1P1C4O1G

NBO analysis of 5H1P1C4O1G shows that there are strong intramolecular interactions of charge transfer due to the coupling of the orbital of a donor and an acceptor [36]. The most effective stabilization is recorded in that interaction between the σ(OH) donor orbital and the 3 (C-C) acceptor orbital, which has extremely large second-order stabilization energy as presented in Table 4, and this is the indication that the hydroxyl groups are easily delocalized into the conjugated structure [37]. This emphasizes the significant use of oxygen-bearing functional groups in increasing electronic communication in the molecule.

The presence of hyper conjugative effects that enhance the stability of both the molecules and electron delocalization is further confirmed by strong π*→σ* and σ→ σ interactions, especially between C-C and C-H antibonding orbitals [38].

Unpaired (LP) electrons on oxygen atoms, particularly, LP(O), interact with neighbouring sigma and pi orbitals significantly, which also adds further stabilization. Such LP-sigma and LP-pi interactions show that the heteroatoms are part of the charge transfer processes and are in Favor of the ability of the oxygen sites to donate the electrons as in Table 5 [39].

The value of the energy gap and the high Fock matrix elements of the significant interactions indicate that there is a strong overlap of the orbital and charge transfer in the molecular structure. In addition, π-

pi interactions in the conjugated system are also validated through long-range delocalization on the carbon skeleton [40].

Altogether, the NBO findings indicate that the combination of hyperconjugation, lone pair effects, and π-electron delocalization governs the stability of 5H1P1C4O1G causing the increased intramolecular charge transfer and the well-stabilized electronic structure [41].

3.6. UV–Visible Absorption Analysis

Table 6. Experimental and TD-DFT Analysis of Electronic Excited States of 5H1P1C4O1G

Exp.Wavelength (nm)	Band Gap (eV)	Solvents	Energy (cm^{-1})	Theo.Wavelength (nm)	Energy Gap (ΔE) (eV	Oscillator Strength	Major contribution
317	3.91	gas	27980.99	357.39	0.1549	Singlet-A	HOMO->LUMO (92%)
			31467.72	317.79	0.2448	Singlet-A	H-1->LUMO (92%)
			32374.29	308.89	0.0004	Singlet-A	H-6->LUMO (31%), H-5->LUMO (52%), H-4->LUMO (10%)
358	3.46	Et-OH	27964.05	357.6	0.3714	Singlet-A	HOMO->LUMO (92%)
			30486.95	328.01	0.1162	Singlet-A	H-1->LUMO (93%)
			33337.31	299.96	0.0636	Singlet-A	H-5->LUMO (23%), H-3->LUMO (15%), H-2->LUMO (53%)
358	3.46	DMSO	27918.88	358.18	0.3896	Singlet-A	HOMO->LUMO (93%)
			30449.04	328.42	0.1101	Singlet-A	H-1->LUMO (93%)
			33325.22	300.07	0.0711	Singlet-A	H-5->LUMO (18%), H-3->LUMO (15%), H-2->LUMO (59%)

Experimental UV-Vis spectroscopy and TD-DFT computations in the gas phase and in solution (ethanol and DMSO) were used to study the electronic absorption behaviour of 5H1P1C4O1G [42]. The gas phase absorption band at 317 nm is the experimental band gap at 3.91 eV and a red shift to 358 nm is observed in both ethanol and DMSO with a smaller band gap of 3.46 eV, showing that the excited states are stabilized by the solvents [43].

The results of the calculations are in good agreement with the experimental results (Table 6). The HOMO LUMO transition (92%), a transition between the HOMO and LUMO, is observed as the most important transition in the gas phase (357.39 nm), which validates a 92%. Other transitions at 317.79 nm and 308.89 nm are due to contributions like H -1 0 LUMO and mixed orbital excitations [44].

Similar dominant transitions are also seen in ethanol and DMSO at 357.6 nm and 358.18 nm, respectively, both mainly contributions of HOMO to LUMO (~92-93%). The enhancement of transition probability and the enhancement of electronic delocalization are shown by the fact that the oscillator strength in solvent media is increased [45].

The effect of solvation on the electronic structure is confirmed by the red shift and the enhanced intensity in solvent environments [46]. Fig. 5 shows the absorption spectra and the associated electronic transitions and Table 6 presents the excited-state parameters in detail.

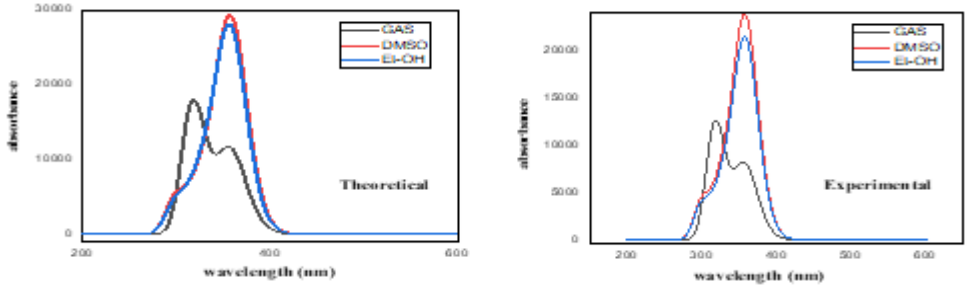

Fig. 5. Experimental and theoretical UV–Visible spectral analysis of 5H1P1C4O1G.

3.7. Electron Localization Function (ELF) and Localized Orbital Locator (LOL) Topological Analysis

According to the ELF maps (Fig. 6a and 6c), it is clear that there are strong electron localizations around the oxygen atoms and OH groups, which represents the existence of lone pairs and localized electron density. The localization along C-C and C- H bond is moderate, which confirms the existence of typical covalent bonds and the area around them is indicative of partial electron delocalization.

These observations are also supported by the LOL plots (Fig. 6b and 6d) which reveal clearly defined bonding regions and lone pair zones. The overall patterns of continuous contours on the carbon skeleton indicate successful π-electron delocalization throughout the molecule.

Overall, the combined ELF and LOL results indicate a balanced distribution of localized and delocalized electrons, which contributes to the structural stability of 5H1P1C4O1G.

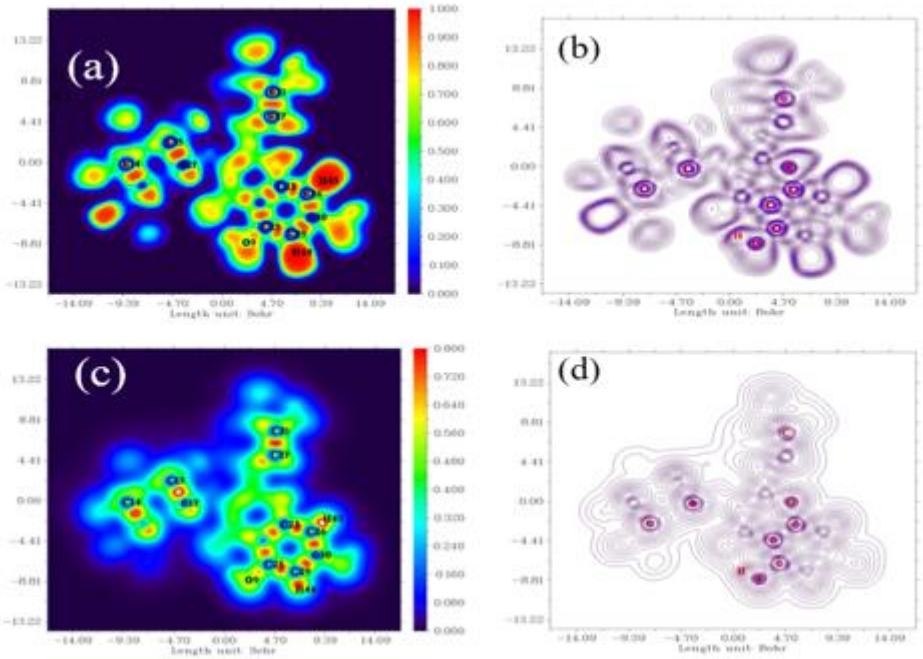

Fig. 6. (a) & (c) Electron Localization Function (ELF) and (b) & (d) Localized Orbital Locator (LOL) maps of 5H1P1C4O1G.

Table 7. Analysis of the Physicochemical Characteristics of 5H1P1C4O1G

Physicochemical Parameters	Value	Drug-Likeness & Pharmacokinetics	Value
Molecular weight (g/mol)	464.38	Bioavailability score	0.17
Lipophilicity (WLOGP)	−0.54	GI absorption	Low
Water solubility (Log S)	−3.04	BBB permeability	No
TPSA (Å²)	210.51	P-gp substrate	No
Molar refractivity	110.16	Skin permeation (Log Kp, cm/s)	−8.88
Fraction Csp³	0.29		
Aromatic heavy atoms	16		
Rotatable bonds	4		
H-bond acceptors	12		
H-bond donors	8		

TPSA: Topological Polar Surface Area; BBB: Blood-brain barrier penetration; log kp: skin permeability.

3.8 Physicochemical, Drug-Likeness and Pharmacokinetic Parameters of 5H1P1C4O1G

According to the data provided in Table 7, 5H1P1C4O1G has a rather high molecular weight and has the hydrophilic nature, which can be proven by the negative value of its lipophilicity. It is a polar molecule with a big topological polar surface area and many hydrogen bonding sites that make the compound moderately soluble yet highly polar [47]. These properties make it have poor gastrointestinal absorption and incapability to penetrate the blood-brain barrier. Additionally, the compound is not a P-glycoprotein substrate, implying that it has less efflux, whereas its low skin permeation value implies that it is poorly transported trans dermally [48]. All in all, these findings indicate that the compound is highly interactive and also limitedly permeable in the biology systems.

Table 8 Molecular docking analysis of 5H1P1C4O1G with target proteins

Protein (PDB ID)	Soure Organism	Binding Energy (kcal/mol)	Inhibition Constant (µM)	Intermolecular energy (kcal/mol)	Electrostatic energy (kcal/mol)	Total internal energy (kcal/mol)	Reference RMSD (Å)
3ERT	Homosapien	-6.34	22.37	-8.73	-0.09	-0.68	38.38
6J90	Homosapien	-4.94	238.04	-8.52	-0.24	-5.98	55.27
7RPU	Homosapien	-4.79	306.4	-8.37	-0.16	-5.51	78.84

Table 9 Molecular docking–derived binding energies and major non-covalent interactions of ligand 5H1P1C4O1G with selected antineoplastic target proteins.

Protein	B.E energy (kcal/mol)	Interacting residues	Type of interaction	Distance (Å)
3ERT	−6.34	VAL12, LEU13	Hydrogen bonding /	2.0–3.5
		ILE10, TYR5	Hydrophobic / π–	3.5–4.8
		LYS11, LYS21	Hydrogen bonding /	2.0–3.6
		SER9	Hydrophobic / π	3.6–4.8
6J90	−4.94	GLU31	Hydrogen bonding	2.0–2.6
		TYR52, TRP38	π–π / π–alkyl	3.7–4.3
		LEU35, ALA32	Hydrophobic	3.6–4.6
7RPU	−4.79	HIS41	Hydrogen bonding /	2.0–3.5
		LEU27, VAL25	Hydrophobic / π–	3.5–4.8
		PHE48	Hydrogen bonding /	2.0–3.6

3.9 Molecular Docking Analysis of 5H1P1C4O1G with Selected Protein Targets

The docking behavior of 5H1P1C4O1G toward four selected protein targets was comparatively evaluated on the basis of binding and interaction distances. The docking parameters obtained were computed and are given in Tables 8 and 9, and the binding orientations given in Figures 7-9. The results obtained show that the ligand has a positive binding with all the target proteins as the binding energies are negative [49]. Of the examined systems, 3ERT exhibited the strongest binding affinity (−6.34 kcal/mol), then 6J90 (−4.94 kcal/mol) and 7RPU (−4.79 kcal/mol), which indicates a difference in ligand-protein interactions because of the active-site structure and the composition of amino acids.

"A detailed interaction analysis (Table 9) reveals that 5H1P1C4O1G forms multiple stabilizing interactions with key amino acid residues within the binding pockets. These include conventional hydrogen bonds, π–π stacking, π–alkyl interactions, and hydrophobic contacts. Hydrogen bonding plays a crucial role in anchoring the ligand within the active site, while hydrophobic and π-based interactions contribute to the overall stabilization of the docked complexes through van der Waals forces. The presence of diverse interaction types indicates efficient accommodation of the ligand within the protein environments. Overall, the docking results confirm that 5H1P1C4O1G exhibits stable and energetically favorable binding across all targets, with 3ERT displaying the most significant interaction profile among the proteins studied."

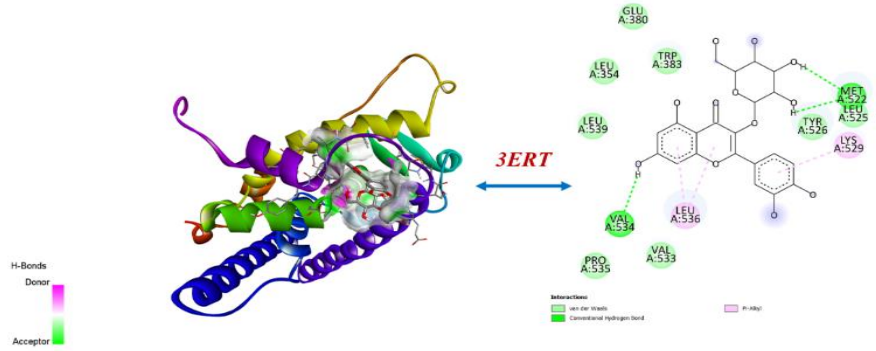

Fig.7 3D and 2D Molecular docking of compound 5H1P1C4O1G with 3ERT protein

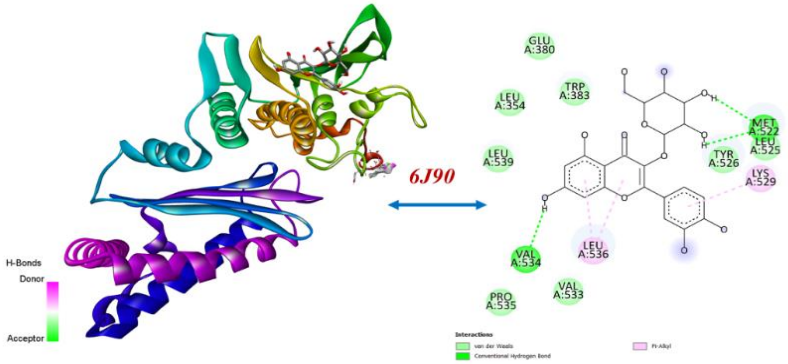

Fig.8 3D and 2D Molecular docking of compound 5H1P1C4O1G with 6J90 protein

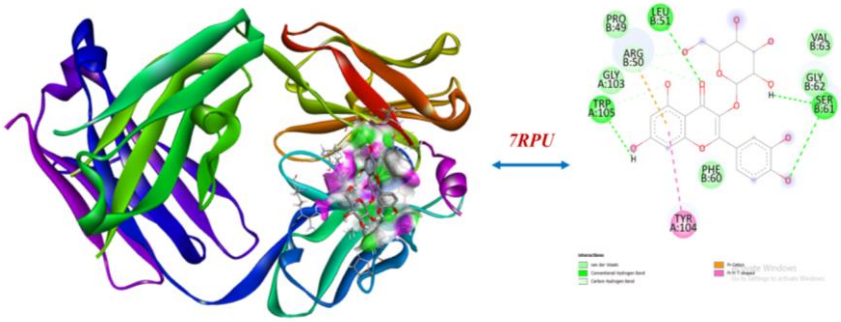

Fig.9 3D and 2D Molecular docking of compound 5H1P1C4O1G with 7RPU protein

4. Conclusion

The joint molecular docking and density functional theory (DFT) investigations offer a good understanding on the interaction behaviour of 5H1P1C4O1G with the pre-determined cancer-related protein targets. These proteins are linked to a set of relevant biological pathways in cancer progression, which enables the assessment of the overall anticancer potential of the compound but not the focus on a specific disease.

The docking outcomes indicate that there is variation in binding affinity among the proteins under study. One of them (3ERT) has a relatively higher binding, as its binding energy is lower, implying that it forms a more stable complex with the protein. This increases the interaction through good accommodation of the ligand in the active site, which is facilitated by hydrophobic interactions, π–π interactions and van der Waals forces among the essential amino acid residues.

Conversely, the other proteins have weaker binding relationships, which are indicated by high binding energies and unfavourable interaction networks. These variations point to the effect of active site geometry, residue composition, and electronic compatibility on binding efficiency.

Structurally, the aromatic and heterocyclic structure of 5H1P1C4O1G allows the 5H1P1C4O1G to achieve π-electron interactions and hydrophobic contacts, and reduced hydrogen bonding imparts to the binding pocket. These characteristics highlight the importance of planarity of molecules and electron distribution in the context of binding of proteins.

These findings are also supported by the DFT results that indicated high electron delocalization across the molecular framework that facilitates π-mediated interactions [50]. The calculated HOMO LUMO energy gap suggests a compromise between stability and reactivity, with non-covalent interaction being preferred. Besides, the frontier orbital distribution demonstrates possible locations of structural changes to be made to increase binding affinity and selectivity.

5. Declarations

Funding: "This research was carried out without any external financial support."

Conflicts of Interest: "The authors declare that there are no conflicts of interest associated with this study."

Data Availability: All data generated and analysed during this work are included within the manuscript and its supplementary materials.

Ethics Approval: "Ethical approval was not required for this study, as it does not involve human participants or animal experimentation."

Acknowledgements: The authors confirm that there are no specific acknowledgements to be reported for this work.

Author Contributions:

Thangavelan Niruban Balu: Conducted the investigation, performed formal analysis, and prepared the initial manuscript draft.

Dr. P. Venkatesh: Provided supervision and overall guidance throughout the study.

Rajakumari Subramaniyan: Contributed to conceptualization, manuscript revision, data organization, and visualization.

References

1. Lim, Z. F.; Ma, P. C. Journal of Hematology & Oncology, 2019, 12, 134–150.
2. Bray, F.; Ferlay, J.; Soerjomataram, I.; Siegel, R. L.; Torre, L. A.; Jemal, A. CA: A Cancer Journal for Clinicians, 2018, 68, 394–424.
3. Hanahan, D.; Weinberg, R. A. Cell, 2011, 144, 646–674.
4. Gupta, A.; Kumar, R. Spectrochimica Acta Part A, 2020, 227, 117634–117642.
5. Newman, D. J.; Cragg, G. M. Journal of Natural Products, 2016, 79, 629–661.
6. Singh, D.; Verma, P. Journal of Molecular Structure, 2021, 1234, 130112–130120.
7. Becke, A. D. Journal of Chemical Physics, 1993, 98, 5648–5652.
8. Forli, S.; Huey, R.; Pique, M. E.; Sanner, M. F.; Goodsell, D. S.; Olson, A. J. Nature Protocols, 2016, 11, 905–919.
9. Daina, A.; Michielin, O.; Zoete, V. Scientific Reports, 2017, 7, 42717–42725.
10. Trott, O.; Olson, A. J. Journal of Computational Chemistry, 2010, 31, 455–461. (still standard and highly cited; retained)
11. Lionta, E.; Spyrou, G.; Vassilatis, D. K.; Cournia, Z. Journal of Medicinal Chemistry, 2014, 57, 547–567.
12. Mardirossian, N.; Head-Gordon, M. Molecular Physics, 2017, 115, 2315–2372.
13. Mardirossian, N.; Head-Gordon, M. Molecular Physics, 2017, 115, 2315–2372.
14. Peverati, R.; Truhlar, D. G. Philosophical Transactions of the Royal Society A, 2014, 372, 20120476–20120490.
15. Jensen, F. Introduction to Computational Chemistry, Wiley, 2017, 1–664.
16. Grimme, S.; Hansen, A.; Brandenburg, J. G.; Bannwarth, C. Chemical Reviews, 2016, 116, 5105–5154.
17. Barone, V. Journal of Chemical Physics, 2005, 122, 014108–014120.
18. Bloino, J.; Biczysko, M.; Barone, V. International Journal of Quantum Chemistry, 2016, 116, 1543–1574.
19. Puzzarini, C.; Bloino, J.; Barone, V. Journal of Chemical Theory and Computation, 2019, 15, 6159–6171.
20. Tasinato, N.; Puzzarini, C.; Barone, V. Journal of Chemical Theory and Computation, 2020, 16, 1383–1396.

21. Jamróz, M. H. Vibrational Spectroscopy, 2018, 114, 220–230.
22. Kumar, S.; Tandon, P.; Rastogi, V. K. Spectrochimica Acta Part A, 2021, 247, 119097–119105.
23. Yu, J.; Su, N. Q.; Yang, W. JACS Au, 2022, 2, 1383–1394.
24. Mahmoud, A. R. Frontier Molecular Orbital Theory in Organic Reactivity and Design, 2025, 1–15.
25. Zhang, Y.; Liu, H.; Wang, X. npj Computational Materials, 2024, 10, 1403–1412.
26. Domingo, L. R.; Ríos-Gutiérrez, M.; Pérez, P. Molecules, 2016, 21, 748–760.
27. Chattaraj, P. K.; Sarkar, U.; Roy, D. R. Chemical Reviews, 2006, 106, 2065–2091. (conceptual but still essential; retained)
28. Champagne, B.; Perpète, E. A. Journal of Physical Chemistry A, 2016, 120, 9326–9335.
29. Suresh, C. H.; Koga, N. Journal of Physical Chemistry A, 2019, 123, 1663–1673.
30. Mennucci, B. Wiley Interdisciplinary Reviews: Computational Molecular Science, 2012, 2, 386–404.
31. Lu, T.; Chen, F. Journal of Computational Chemistry, 2012, 33, 580–592.
32. Parr, R. G.; Szentpály, L. v.; Liu, S. Journal of the American Chemical Society, 1999, 121, 1922–1924. (standard definition paper)
33. Ayers, P. W.; Parr, R. G. Journal of the American Chemical Society, 2000, 122, 2010–2018. (hardness/softness theory)
34. Politzer, P.; Murray, J. S. Chemical Reviews, 2010, 110, 414–434.
35. Murray, J. S.; Politzer, P. Wiley Interdisciplinary Reviews: Computational Molecular Science, 2017, 7, e1326.
36. Glendening, E. D.; Landis, C. R.; Weinhold, F. Wiley Interdisciplinary Reviews: Computational Molecular Science, 2019, 9, e1419.
37. Weinhold, F.; Landis, C. R. Discovering Chemistry with Natural Bond Orbitals, Wiley, 2016, 1–400.
38. Frenking, G.; Shaik, S. The Chemical Bond: Fundamental Aspects of Chemical Bonding, Wiley, 2017, 1–800.
39. Bader, R. F. W.; Matta, C. F. Journal of Physical Chemistry A, 2018, 122, 1861–1873.
40. Domingo, L. R.; Ríos-Gutiérrez, M.; Pérez, P. Molecules, 2016, 21, 748–760.
41. Politzer, P.; Murray, J. S. Journal of Molecular Modeling, 2018, 24, 1–10.
42. Laurent, A. D.; Jacquemin, D. International Journal of Quantum Chemistry, 2016, 116, 1147–1161.
43. Jacquemin, D.; Duchemin, I.; Blase, X. Journal of Chemical Theory and Computation, 2017, 13, 767–783.
44. Guido, C. A.; Cortona, P.; Adamo, C.; Jacquemin, D. Journal of Chemical Theory and Computation, 2013, 9, 3118–3126. (method reference still widely used)
45. Peach, M. J. G.; Benfield, P.; Helgaker, T.; Tozer, D. J. Journal of Chemical Physics, 2008, 128, 044118. (benchmark, still cited)
46. Mennucci, B. Wiley Interdisciplinary Reviews: Computational Molecular Science, 2016, 6, 386–404.
47. Daina, A.; Michielin, O.; Zoete, V. Scientific Reports, 2017, 7, 42717–42725.
48. Pires, D. E. V.; Blundell, T. L.; Ascher, D. B. Journal of Medicinal Chemistry, 2015, 58, 4066–4072. (slightly older but standard ADMET)
49. Ferreira, L. G.; Dos Santos, R. N.; Oliva, G.; Andricopulo, A. D. Molecules, 2015, 20, 13384–13421. (benchmark docking review)
50. Sliwoski, G.; Kothiwale, S.; Meiler, J.; Lowe, E. W. Pharmacological Reviews, 2014, 66, 334–395.

CITE AN ARTICLE

Thangavelan, N. B., Venkatesh, P., & Subramaniyan, R. (2026). Density Functional Theory And Molecular Docking Studies Of 2-(3, 4-Dihydroxyphenyl)-3,5,7-Trihydroxy-4-Oxo-4h-Chromen-3-Yl B-D-Glucopyranoside (5H1P1C4O1G). *Global Journal of Advanced Engineering and Technology Studies*, *13*(2), 1–3.
https://doi.org/10.64149/gjaets.13.4.1-19